

# **Geophysical Research Letters**

# RESEARCH LETTER

10.1029/2025GL116392

### **Key Points:**

- · Northeast-southwest aligned wavefronts of electrified medium-scale traveling ionospheric disturbance (EMSTID) observed in detrended total electron content maps
- Disturbance dynamo-driven electric field and wind provided favorable conditions to initiate Perkins instability that generated the EMSTID
- Eastward/westward penetration electric field in mid-latitude ionosphere associated with expansion/recovery phase of a substorm

#### **Supporting Information:**

Supporting Information may be found in the online version of this article.

#### Correspondence to:

D. Patgiri. dipjyoti\_p@ph.iitr.ac.in

### Citation:

Patgiri, D., Otsuka, Y., Shreedevi, P. R., Kakoti, G., Ranjan, A. K., Rathi, R., et al. (2025). Unusual phase alignment of nighttime electrified medium-scale traveling ionospheric disturbance after moderate geomagnetic storms and response to substorms. Geophysical Research Letters 52 e2025GL116392 https://doi.org/10.1029/2025GL116392

Received 9 APR 2025 Accepted 6 OCT 2025

## **Author Contributions:**

Conceptualization: Dipjyoti Patgiri,

Yuichi Otsuka

Data curation: Yuichi Otsuka, Atsuki Shinbori, Michi Nishioka, Septi Perwitasari

Formal analysis: Dipjyoti Patgiri, Yuichi Otsuka, P. R. Shreedevi, Geetashree Kakoti, Alok Kumar Ranjan,

Rahul Rathi

Funding acquisition: Yuichi Otsuka Investigation: Yuichi Otsuka Methodology: Dipjyoti Patgiri, Yuichi Otsuka, P. R. Shreedevi Project administration: Yuichi Otsuka

© 2025. The Author(s). This is an open access article under the terms of the Creative Commons Attribution License, which permits use, distribution and reproduction in any medium, provided the original work is properly cited.

# Unusual Phase Alignment of Nighttime Electrified Medium-**Scale Traveling Ionospheric Disturbance After Moderate** Geomagnetic Storms and Response to Substorms

Dipjyoti Patgiri<sup>1,2</sup>, Yuichi Otsuka<sup>2</sup>, P. R. Shreedevi<sup>2</sup>, Geetashree Kakoti<sup>2</sup> Alok Kumar Ranjan<sup>3</sup>, Rahul Rathi<sup>4</sup>, Atsuki Shinbori<sup>2</sup>, Michi Nishioka<sup>5</sup>, and Septi Perwitasari<sup>5</sup>

<sup>1</sup>Department of Physics, Indian Institute of Technology Roorkee, Roorkee, India, <sup>2</sup>Institute for Space-Earth Environmental Research, Nagoya University, Nagoya, Japan, <sup>3</sup>Physical Research Laboratory, Space and Atmospheric Sciences Division, Ahmedabad, India, <sup>4</sup>Physics Department, Lancaster University, Lancaster, UK, <sup>5</sup>National Institute of Information and Communications Technology (NICT), Tokyo, Japan

**Abstract** A nighttime electrified medium-scale traveling ionospheric disturbance (EMSTID) was observed over Japan on 17 March 2003, after two moderate geomagnetic storms. Unlike typical northwest-southeast alignment in quiet conditions, the EMSTID exhibited an unusual northeast-southwest orientation. Challenging Minisatellite Payload neutral wind and ROCSAT-1 ion drift measurements showed significant thermospheric wind and electric field variations from quiet-times. The study reveals a unique disturbance dynamo-driven electrodynamical mechanism that triggers Perkins instability, generating unusually aligned nighttime EMSTID. Notably, low electron density and weak inhomogeneity in sporadic-E layers in both locally (Wakkanai, Japan) and over conjugate regions (Townsville, Australia) reveal that Perkins instability can be enhanced sufficiently to generate EMSTIDs, even with weak E-F regions coupling within or across hemispheres. Additionally, penetration electric fields during a substorm's expansion and recovery phases instantaneously modulated EMSTID amplitudes. Such nighttime EMSTID, comprising unique features and near-instantaneous amplitude modulation caused by substorm-induced electric fields, represents the novel observation of this study.

Plain Language Summary Plasma instabilities, driven by different forcings, give rise to density irregularities in the Earth's ionosphere that significantly disrupt trans-ionospheric radio wave propagation, thereby affecting space-based communication and navigation systems. Among these irregularities, mediumscale traveling ionospheric disturbances (MSTIDs) are quasi-periodic perturbations in F-region plasma density, typically characterized by horizontal wavelengths of a few hundred kilometers. Nighttime MSTIDs in the northern hemisphere typically exhibit a northwest-southeast alignment and propagate southwestward, often generated through Perkins instability seeded by E-F region coupling, and are commonly known as electrified MSTIDs (EMSTIDs). Northeast-southwest aligned EMSTID was observed in detrended total electron content maps over Japan on 17 March 2003, following two moderate geomagnetic storms. A comparative analysis of thermospheric wind and vertical ion drift measurements between the storm day and quiet days revealed significant storm-time modifications in both wind and electric fields. These disturbed conditions likely created a favorable environment for the growth of Perkins instability, leading to the generation of the atypically aligned EMSTID. Interestingly, ionosonde observation revealed that Perkins instability is sufficiently enhanced to generate EMSTIDs, even with weak E-F region coupling within or across hemispheres. Additionally, EMSTID amplitudes showed instantaneous modulation with substorm's expansion/recovery phases, suggesting the penetration of electric fields.

### 1. Introduction

Medium-scale traveling ionospheric disturbances (MSTIDs) are wave-like undulations in F-region plasma density with horizontal wavelengths within 100-400 km, velocities within 50-200 m/s, and periods of few hours (Duly et al., 2013; Garcia et al., 2000; Hunsucker, 1982). Previously, studies reported that MSTIDs can be classified into daytime, nighttime, dusk, and dawn MSTIDs based on their local time of occurrence, noting that each type is typically driven by distinct generation mechanisms (Otsuka et al., 2011; Perwitasari et al., 2022; Tsugawa et al., 2007). In the northern hemisphere over mid-latitudes, nighttime MSTID wavefronts are mostly northwest-southeast (NW-SE) oriented with southwest (SW) propagation direction during geomagnetic quiet

PATGIRI ET AL. 1 of 11



Supervision: Yuichi Otsuka

Writing – original draft: Dipjyoti Patgiri, Yuichi Otsuka, P. R. Shreedevi, Geetashree Kakoti, Alok Kumar Ranjan, Rahul Rathi Writing – review & editing: Dipjyoti Patgiri, Yuichi Otsuka, P. R. Shreedevi, Geetashree Kakoti, Alok Kumar Ranjan, Rahul Rathi conditions (Ding et al., 2011; Otsuka et al., 2011; Shiokawa, Ihara, et al., 2003; Tsugawa et al., 2007). Perkins instability, reinforced by E–F region coupling, is the primary generation mechanism of nighttime MSTIDs, accounting for their preferential alignment and electrical nature, commonly referred to as electrified MSTIDs (EMSTIDs) (Hamza, 1999; M. Kelley et al., 2003; M. C. Kelley et al., 2003; Perkins, 1973; Shiokawa, Otsuka, et al., 2003).

The generation mechanism of MSTIDs during geomagnetic storms is an unresolved research topic. Previously, a limited number of studies documented the occurrence of nighttime MSTIDs during geomagnetic storms, particularly over mid- to high-latitude regions of the northern hemisphere (I. J. Kelley et al., 2023; Y. Liu et al., 2020; Nishioka et al., 2009; Zhang et al., 2019, 2022). They suggested different factors that can trigger the generation of MSTIDs, viz. electric field associated with subauroral polarization stream (SAPS), gravity wave caused by ion-neutral frictional heating due to SAPS flow, prompt penetration electric field (PPEF), and disturbance dynamo electric field (DDEF). These MSTIDs typically exhibit NW-SE orientation, which aligns with the characteristics of quiet-time nocturnal MSTIDs.

Another important phenomenon that can extensively affect the dynamics of magnetosphere-ionosphere (MI) system are substorms. Although substorms are primarily localized in the nightside, their effects can extend throughout the entire MI system, influencing global convection through processes like magnetotail reconnection and dipolarization (Huang et al., 2004; Kikuchi et al., 2003; Sastri et al., 2003). However, precise role of substorms in driving either eastward or westward electric fields at low and mid-latitudes remains a topic of debate, as both directions have been observed (Chakrabarty et al., 2010, 2015; Gonzales et al., 1979; Huang, 2009; Huang et al., 2004; Hui et al., 2017; Kikuchi et al., 2003; Sastri et al., 2003; Sibeck et al., 1998). Rathi et al. (2025) were the first to report variations in EMSTID amplitudes linked to substorms. They observed expected typical alignment, that is, NW-SE, with a delayed response characterized by an amplitude increase during one substorm onset and a decrease during another.

Contrary to the findings of Rathi et al. (2025) and other reported storm-time EMSTID event studies, northeast-southwest (NE-SW) aligned EMSTID was observed on 17 March 2003 over Japan following two moderate storms. This distinctive NE-SW alignment of nighttime EMSTIDs over mid-latitudes is an important and novel observation, as it challenges the existing understanding and highlights the previously underexplored aspects of ionospheric dynamics. Furthermore, the atypically aligned EMSTID showed simultaneous enhancement/reduction in its amplitudes during the expansion/recovery phase of a substorm. This study provides valuable insights into the complex interactions between substorms and ionospheric disturbances, paving the way for further investigations into the behavior of EMSTIDs during geomagnetic events.

# 2. Instruments and Data Analyses

Detrended total electron content (DTEC) maps have been used to examine the spatiotemporal evolution of TEC perturbations caused by the MSTID on 17 March 2003. TEC data are obtained from over 1,000 dual-frequency (1.57542 and 1.22760 GHz) GPS receivers in Japan operated by the Geospatial Information Authority of Japan. Detailed procedure of TEC calculation (at 30-s intervals) and DTEC maps have been described in multiple literature (e.g., Otsuka et al., 2002; A. Saito et al., 1998). After subtracting 1-hr running average ( $\pm$ 30 min centered on each) of TEC from the original TEC series for PRNs 2, 4–6, 8, 10, 14–18, 23–27, 29–30, with conversion of slant to vertical TEC, DTEC maps were constructed with a spatial resolution of 0.15° × 0.15° in latitude-longitude (with 7 × 7 pixel smoothing) considering an ionospheric shell at 300 km. TEC amplitude perturbations caused by MSTIDs were determined by calculating the standard deviation of DTEC values within the region 137.95°E–144.1°E, 37°N–44.55°N, which lies within the MSTID observation region. This region covers at least one full MSTID wave (100–400 km) over Japan (Otsuka et al., 2011; Shiokawa, Ihara, et al., 2003).

Interplanetary parameters, time-shifted to the Earth's bow shock nose, were obtained from the High-Resolution OMNI data set. The time lag between the subsolar bow shock and ionosphere was further corrected using the method described by Chakrabarty et al. (2005).

F-layer base height (h'F) variations were studied using manually scaled 15-min resolution data from ionosondes located in Wakkanai (45.39°N, 141.69°E), Kokubunji (35.71°N, 139.49°E), Yamagawa (31.20°N, 130.62°E), and Okinawa (26.68°N, 128.16°E) in Japan. To examine sporadic-E ( $E_S$ ) activity, manually scaled 15-min resolution  $f_OE_S$  and  $f_bE_S$  data (critical and blanketing frequencies of the  $E_S$  layers) from Wakkanai, along with hourly

PATGIRI ET AL. 2 of 11



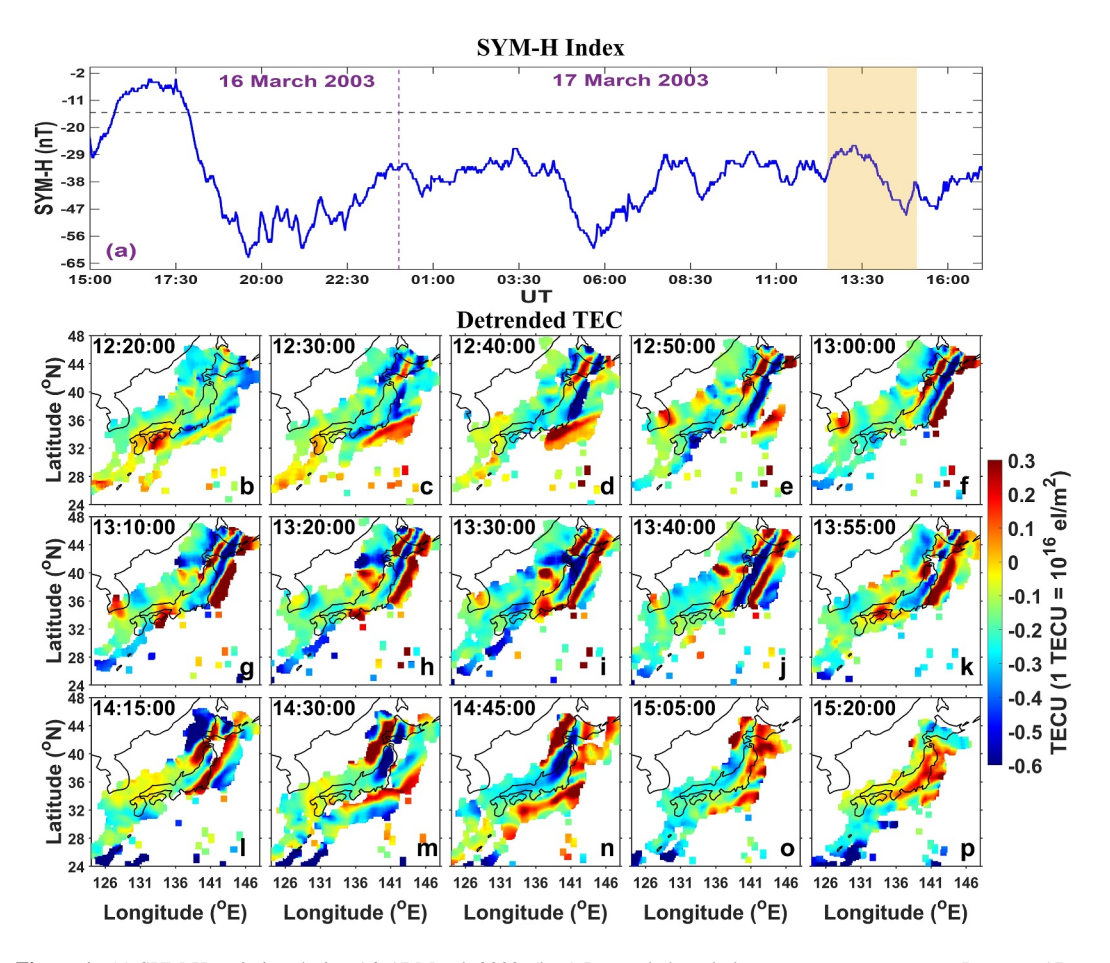


**Figure 1.** (a) SYM-H variation during 16–17 March 2003. (b–p) Detrended total electron content maps over Japan on 17 March 2003. Shaded area in panel (a) represents the duration of medium-scale traveling ionospheric disturbance observation.

manually scaled data from the geomagnetic conjugate station, Townsville (19.3°S, 146.7°E), Australia, were utilized.

Thermospheric zonal and meridional winds were derived from in situ cross-track wind measurements of the accelerometer, Spatial Triaxial Accelerometer for Research onboard the Challenging Minisatellite Payload (CHAMP) satellite (H. Liu et al., 2006; Reigher et al., 2002).

Additionally, to examine vertical ion drifts over mid-latitudes, 1s-averaged ion drift data of Ionospheric Plasma and Electrodynamics Instrument, onboard ROCSAT-1 satellite were used.

### 3. Results

# 3.1. EMSTID With Northeast-Southwest (NE-SW) Aligned Phase Fronts Following Two Geomagnetic Storms

Figure 1a shows SYM-H index during 16–17 March 2003, highlighting two moderate geomagnetic storms: first began with a drop after 17:30 UT on 16 March, reaching minimum (–63 nT) by 19:37 UT. While the second occurred as SYM-H values were still recovering from the first storm, marked by another dip to –60 nT at 05:41 UT on 17 March. According to the Joint USAF/NOAA Report, both storms were likely driven by a coronal hole high-speed stream, making these days geomagnetically active (daily averaged Kp = 3.9 and 4.7, Ap = 31 and 42). Figures 1b–1p represent DTEC maps over Japan on the night of 17 March 2003, revealing NE-SW aligned wave-like TEC perturbations associated with EMSTIDs, which appeared following the two moderate geomagnetic storms on 16 and 17 March. The duration of EMSTID observation (2.5 hr, 12:30–15:05 UT, LT = UT + 9 hr) is

PATGIRI ET AL. 3 of 11



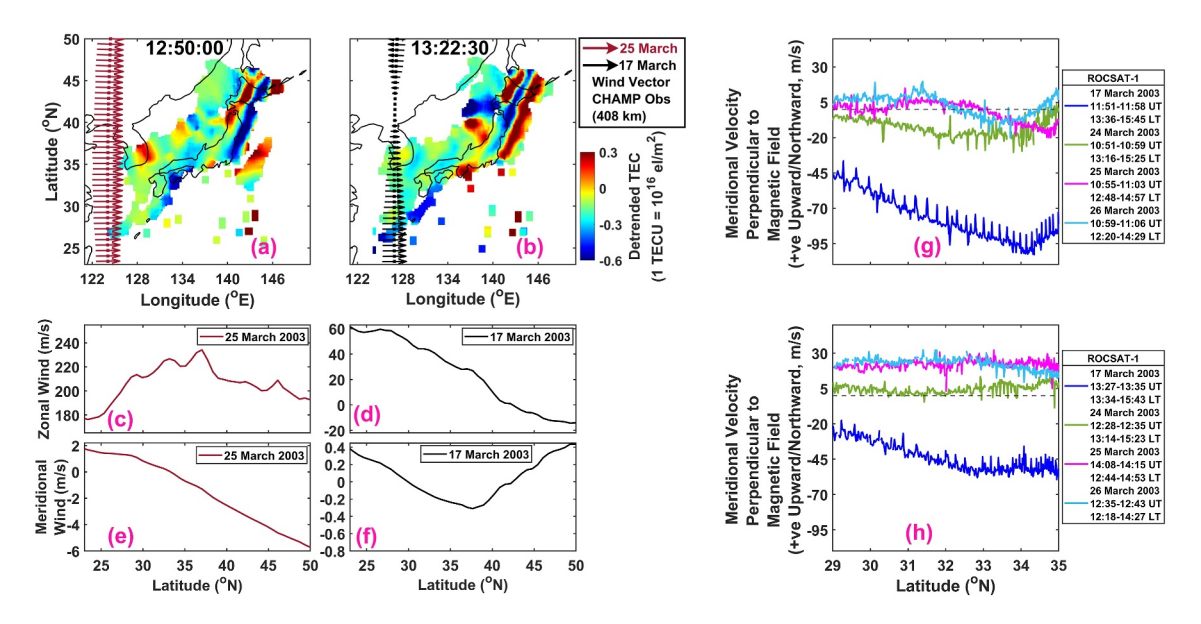


**Figure 2.** Arrows over Detrended total electron content maps (for 17 March) represent CHAMP-measured wind on (a) 25 and (b) 17 March. Latitudinal variations of zonal and meridional winds on (c, e) 25 and (d, f) 17 March. Colored curves in panels (g, h) represent ROCSAT-1 dayside meridional ion drift perpendicular to the magnetic field on 17 and IQDs: 24, 25, and 26 March 2003.

represented by the shaded area in Figure 1a. These TEC perturbations extended latitudinally from  $36^{\circ}N$  to  $46^{\circ}N$  and propagated westward (Figures 1c-10 and Movie S1).

# 3.2. Background Conditions

To examine background thermospheric wind conditions, zonal and meridional winds from CHAMP cross-track measurements at ~408 km on 17 and 25 March (an international quiet day or IQD) are used, shown as vectors over DTEC maps (of 17 March) in Figures 2a and 2b and as latitudinal profiles in Figures 2c–2f. The neutral wind observations on 17 March at 13:22 UT and 25 March at 12:50 UT (Figures 2a and 2b) were selected for their close match in time and location, with both aligned to the period of EMSTID activity observed in the DTEC maps on 17 March. On 25 March, winds were predominantly eastward with minimal meridional component beyond 30°N (Figures 2c and 2e), whereas on 17 March, both zonal and meridional wind magnitudes decreased significantly across all latitudes, with zonal winds turning westward and a weak southward component appearing around the latitudes (>40°N) of EMSTID observation (Figures 2b, 2d, and 2f). Notably, only the wind data from 25 March, the closest IQD to the event date, were used, as they most closely matched the 17 March observations in both time and location during the EMSTID activity.

Figures 2g and 2h present ROCSAT-1 dayside meridional ion velocity (at 570 km) perpendicular to the magnetic field, with blue curves for 17 March and green, magenta, and cyan for IQDs (24–26 March). Prior to EMSTID observation on 17 March, ion velocity was strongly negative, indicating downward/southward drift, while during the same local time on IQDs, values hovered around zero with minor variations (Figure 2g). During EMSTID observation period, ion velocity on 17 March remained persistently downward/southward between 29°N and 35°N, contrasting with slightly to moderately upward/northward motion on IQDs (Figure 2h). Notably, daytime ion drift data alone were selected due to consistent latitudinal (29°N–35°N), local (12:00–16:00 LT), and universal time coverage across all dates.

# 3.3. EMSTID Amplitude Modulations During Substorms With Low Electron Density and Weak Spatial Inhomogeneity in Sporadic-E Layers

Figures 3a–3d represent temporal variations of z-component of the interplanetary magnetic field (IMF-Bz) in GSM coordinates, Auroral Lower index (AL) and SYM-H, h'F from Wakkanai on 17 March, and IQDs on 26 March, 25, 24, and 13 February 2003, h'F on 17 March from Wakkanai, Kokubunji, Yamagawa, and Okinawa, and TEC perturbations amplitude caused by EMSTIDs. Shaded area in Figures 3a–3d denotes EMSTID

PATGIRI ET AL. 4 of 11

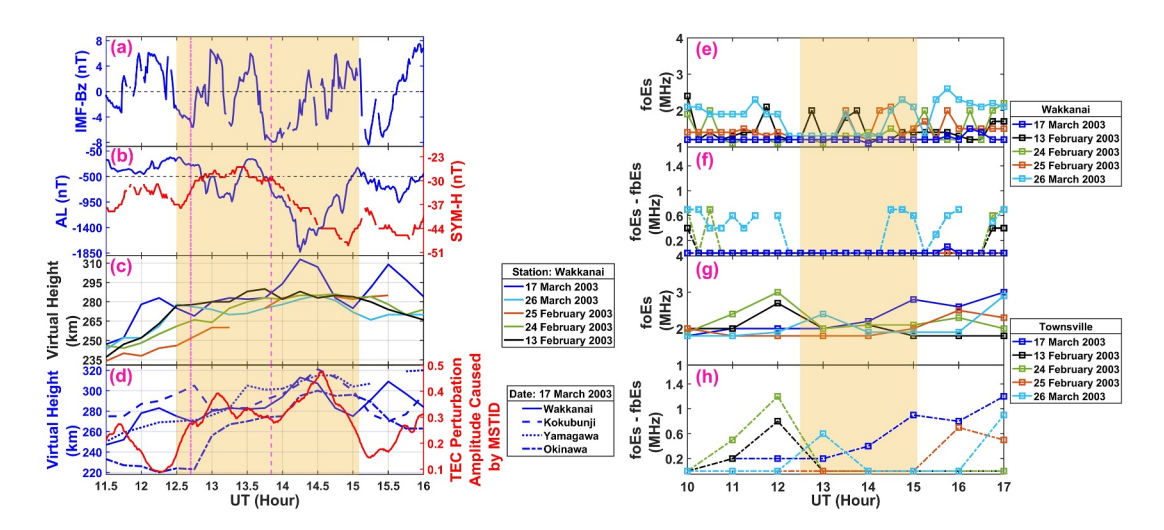


**Figure 3.** Temporal variations of (a) IMF-Bz, (b) AL and SYM-H, (c) h'F from Wakkanai on 17 and 26 March (blue and cyan), 25, 24, and 13 February (orange, green, and black), (d) h'F from Wakkanai (solid), Kokubunji (dashed), Yamagawa (dotted), and Okinawa (dashed-dotted), and electrified medium-scale traveling ionospheric disturbance (EMSTID) amplitude (red-solid) on 17 March. Temporal variations of (e)  $f_0E_S$  and (f)  $f_0E_S$ - $f_0E_S$  on 17, 26 March, 13, 24, 25 February, (g, h) same as (e, f) except at Townsville station with similar color scheme as (c). Vertical lines in panels (a–d) and shaded areas in (a–h) represent onsets of two substorms and EMSTID observation period, respectively.

observation period. Interestingly, two substorms were present during the EMSTID observation, with onsets at 12:42:00 and 13:50:29 UT on 17 March, marked by sudden AL index drops (vertical dashed-dotted and dashed lines). The onset timings were further confirmed by a sudden increase in proton and electron fluxes at various energy levels, as measured by the LANL 1994-084 satellites, as shown in Figure S1 in Supporting Information S1.

During expansion/recovery phases of first substorm on 17 March 2003, h'F at Wakkanai showed no significant variation compared to other quiet nights without any MSTID activity, and responses across stations were not similar; h'F increased at Wakkanai, Yamagawa, and Okinawa but decreased at Kokubunji (Figures 3b–3d). In contrast, during expansion/recovery phases of second substorm, h'F at Wakkanai showed notable enhancement/reduction relative to quiet nights, with simultaneous changes in EMSTID amplitude and h'F observed across all four stations during the expansion/recovery phases. While h'F enhancement/reduction across all stations during expansion/recovery phases of second substorm started around 14 UT/14:30 UT, EMSTID amplitude increased/decreased from 13:58 UT/14:32 UT (Figure 3d).

Figures 3e and 3f denote temporal variations of manually scaled (15-min resolution)  $f_OE_S$  and  $f_OE_S$ - $f_bE_S$ , respectively, at Wakkanai on 17 and 26 March, 13, 24, and 25 February 2003. Figures 3g and 3h are same as Figures 3e and 3f except hourly scaled parameters from a geomagnetic conjugate station, Townsville. During EMSTID observation (shaded area in Figures 3e and 3f),  $f_OE_S$  and  $f_OE_S$ - $f_bE_S$  from Wakkanai on 17 March and quiet nights were significantly lower ( $f_OE_S \le 2.3$  MHz,  $f_OE_S$ - $f_bE_S \le 0.7$  MHz). Notably, as shown in Figures 3g and 3h,  $f_OE_S$  and  $f_OE_S$ - $f_bE_S$  parameters from Townsville were also significantly small across five nights ( $f_OE_S \le 2.8$  MHz,  $f_OE_S$ - $f_bE_S \le 0.9$  MHz).

## 4. Discussion

# 4.1. Generation of EMSTID With Northeast-Southwest Aligned Phase Front

Nighttime MSTID observations during geomagnetically active conditions are rare and mostly reported at mid-to-high latitudes (I. J. Kelley et al., 2023; Y. Liu et al., 2020; Nishioka et al., 2009; Zhang et al., 2019, 2022). These studies reported NW-SE aligned MSTIDs, a typical feature of quiet-time nocturnal MSTIDs in northern hemisphere (Otsuka et al., 2011, 2021; Shiokawa, Ihara, et al., 2003; Tsugawa et al., 2007). However, MSTID observed in this study during geomagnetically active night were NE-SW aligned and propagated westward (Figures 1c–1o), indicating a distinct electrodynamical scenario, distinct from previously proposed mechanisms, highlighting the event's unusual nature.

PATGIRI ET AL. 5 of 11



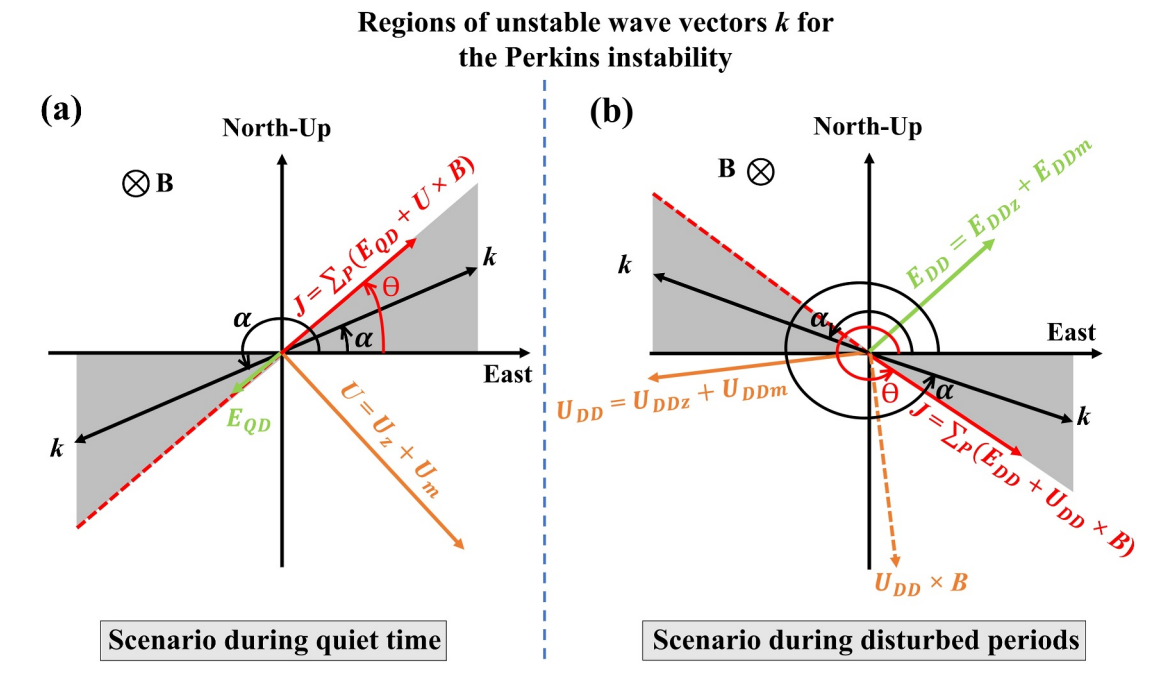


Figure 4. Region of unstable wave-vector for Perkins instability during geomagnetically (a) quiet night and (b) disturbed periods.

Perkins instability is widely considered the primary mechanism for nighttime MSTID generation during geomagnetically quiet periods, as it accounts for their electrical nature, hence the term EMSTIDs and alignment (Hamza, 1999; Perkins, 1973; Shiokawa, Otsuka, et al., 2003). At night, F-region plasma typically balances upward motion from meridional winds and/or  $E \times B$  drift with downward gravitational diffusion (M. Kelley et al., 2003). Plasma density/field-line-integrated Pedersen conductivity ( $\sum_P$ ) perturbations amplify when the wave vector, perpendicular to the perturbation phase front, lies between the east and electric current (Perkins, 1973).

Perkins instability grows only when the perturbation wavevector, k, aligns suitably with respect to the effective electric field ( $E_{\rm eff} = E + U \times B$ ), as described in Equation 1 (Huang et al., 1994; Makela & Otsuka, 2012; Perkins, 1973).

$$\gamma = \frac{|E_{\text{eff}}|\cos D\sin(\Theta - \alpha)\sin \alpha}{BH} = \frac{g\sin^2 D\sin(\Theta - \alpha)\sin \alpha}{\langle \nu_{\text{in}} \rangle H\cos\Theta}$$
(1)

Where D,  $\Theta$ , and  $\alpha$ , H, g, and  $<\nu_{\rm in}>$  represent dip angle, angle between  $E_{\rm eff}$  and geomagnetic east, angle between k and geomagnetic east, atmospheric scale height, gravitational acceleration, and density-weighted height-integrated ion-neutral collision frequency, respectively. Figure 4a shows geomagnetically quiet conditions. During such nights, background southwestward F-region dynamo electric field,  $E_{\rm QD}$  is weaker than the north-eastward  $U \times B$  field induced by southeastward diurnal tide-driven winds ( $U = U_z + U_{\rm m}$ ) in the northern hemisphere (Hedin et al., 1996; Rishbeth, 1971), resulting in a northeastward Pedersen current,  $J = \sum_P (E_{\rm QD} + U \times B) \approx \sum_P (U \times B)$ . Here, subscripts, z and m correspond to zonal and meridional components, respectively. To maintain divergence-free J across  $\sum_P$  perturbations, polarization electric fields ( $E_P$ ) form within them, driving vertical  $E_P \times B$  drifts that amplify the initial perturbations. When k points northeastward or southwestward (shaded area in Figure 4a), the growth rate becomes positive, enabling Perkins instability to generate NW-SE aligned MSTIDs commonly seen during geomagnetically quiet nights over mid-latitudes.

During magnetic storms, direction of background electric field and neutral wind is different from the magnetically quiet condition. CHAMP wind measurement on IQD, 25 March, showed predominantly eastward with minimal meridional component beyond 30°N, while on 17 March, both components weakened across all latitudes, with zonal winds turning westward and weak southward component appearing near latitudes (>40°N) of EMSTID

PATGIRI ET AL. 6 of 11



observation (Figures 2c-2f). Notably, ~2-3 hr after the onset of magnetic storms, dissipating sub-auroral currents and particle precipitation heat the auroral region, building a poleward pressure gradient (equatorward pressure gradient force) driving equatorward meridional winds (Blanc & Richmond, 1980; Fejer et al., 1983, 2008). In the upper thermosphere, where ion-drag plays an important role, neutral wind experiences strong drag forces, causing it to blow across isobars rather than parallel to them (Fujiwara & Miyoshi, 2009; Fuller-Rowell, 1995; Fuller-Rowell et al., 1994). According to Emmert et al. (2004), the westward wind observed over mid-latitudes in the upper thermosphere can be partly attributed to the Coriolis deflection of equatorward winds. Additionally, ion drag forcing plays a significant role, as the storm-time penetration electric fields can drive westward plasma flows that transfer momentum to the neutral atmosphere. However, distinguishing the relative roles of ion drag driven by electrodynamical forcings and Coriolis deflection in neutral wind forcing is challenging (Meriwether, 2008).

According to Blanc and Richmond (1980), westward winds near 150 km drive equatorward/downward Pedersen currents via  $U \times B$ . Due to higher ion collision-to-gyro frequency ratios, ions move slightly while electrons remain nearly stationary, generating equatorward/downward current. To keep the current divergence-free, poleward/upward electric fields (along  $-U \times B$ ) form, driving eastward Hall currents on the dayside (due to the downward/northward B). At night, low conductivity makes Hall currents negligible. Disruption of the dayside Hall current at dusk caused by strong longitudinal density gradients at the terminator, leads to charge accumulation and the formation of a dusk-to-dawn DDEF.

Pronounced negative ion drift on 17 March indicated westward dayside DDEF over mid-latitudes, persisting during the EMSTID event, unlike on other quiet days (Figures 2g and 2h). Although the ion drift measurements indicate the presence of DDEF, no reversal of zonal wind was observed at low latitudes at satellite altitudes (Figure 2d). This discrepancy may be attributed to different wind patterns that likely reversed below ~200 km, the altitude region critical for the formation of disturbed dynamo electric fields (Blanc & Richmond, 1980). Since energy input peaks at lower altitudes (below 150 km) during disturbed times (Richmond, 2021), the likelihood of wind reversal is higher there, consistent with the substantial reduction of eastward winds observed at higher altitudes. Daytime DDEF on 17 March 2003 suggests the possible persistence of eastward DDEF at night, coinciding with the appearance of NE-SW EMSTID phase fronts. At night, eastward/poleward electric fields  $(E_{DDz}/E_{DDm})$  and westward/southward winds  $(U_{DDz}/U_{DDm})$  generated a southeastward Pedersen current,  $J = \sum_P (E_{DD} + U_{DD} \times B)$ , where  $E_{DD} = E_{DDz} + E_{DDm}$  and  $U_{DD} = U_{DDz} + U_{DDm}$  (Figure 4b). This configuration represents an unstable Perkins instability condition after two moderate storms, with the shaded unstable k region in Figure 4b matching the observed NE-SW EMSTID alignment.

Although Perkins instability is the primary generation mechanism of nighttime MSTIDs, its low growth rate and inability to explain preferred propagation directions are major limitations (Garcia et al., 2000; M. C. Kelley & Makela, 2001). Studies have suggested that polarization electric fields within frontal  $E_{\rm S}$  irregularities reinforce Perkins instability, while southwestward propagation results from rotational wind shear in  $E_{\rm S}$  layers (Cosgrove & Tsunoda, 2002; Otsuka et al., 2007; S. Saito et al., 2007; Tsunoda & Cosgrove, 2001; Yokoyama et al., 2009). E-and F-regions are not only coupled in one hemisphere but also with geomagnetic conjugate locations in the other hemisphere, as large-scale polarization electric fields (>10 km) map efficiently between hemispheres (Farley, 1960; La Belle, 1985; Narayanan et al., 2018; Spreiter & Briggs, 1961; Yokoyama, 2014). Parameters like  $f_{\rm O}E_{\rm S}$  and  $f_{\rm O}E_{\rm S}f_{\rm b}E_{\rm S}$ , indicating  $E_{\rm S}$ -layer density and its spatial inhomogeneity strength, show strong correlation with MSTID activity (Otsuka et al., 2008).

To examine  $E_S$  activity on 17 March, we examined temporal variations of  $f_OE_S$  and  $f_OE_S$ - $f_bE_S$  from Wakkanai and geomagnetic conjugate station Townsville, and compared them with four geomagnetically quiet nights without EMSTIDs observation (Figures 3e–3h). Townsville is located in the conjugate region corresponding to the southernmost extent of MSTIDs observed over Japan. Since, both parameters were significantly lower ( $f_OE_S \le 2.8 \text{ MHz}, f_OE_S$ - $f_bE_S \le 0.9 \text{ MHz}$ ) on 17 March at two stations, suggesting weak  $E_S$  activity, we conclude that  $E_S$ -layer polarization electric fields were unlikely to have generated the EMSTID.

In conclusion, the observed NE-SW aligned EMSTID on 17 March 2003 is attributed to a combination of Perkins instability and storm-induced effects, particularly westward winds and associated electric fields generated after storms. Notably, this work shows that Perkins instability can generate EMSTIDs even under conditions of low electron density in  $E_{\rm S}$  layers or when E-F regions coupling is weak in single as well as both hemispheres.

PATGIRI ET AL. 7 of 11



## 4.2. Role of Transient Electric Fields During Substorm in the Variation of EMSTID Amplitude

Over the past few decades, extensive research has been conducted on the effects of PPEFs and shielding electric fields in mid- and low-latitude regions (Fejer et al., 2007, 2008; Gonzalez et al., 1989, 1994; M. Kelley et al., 2003; Tsurutani et al., 2008; and references therein). On the other hand, there have been serious debates on how mid- and low-latitude ionosphere responds to the expansion onset of substorms, particularly in terms of transient electric field penetration. Previous studies have reported both eastward (Chakrabarty et al., 2010; Huang, 2009; Huang et al., 2004; Hui et al., 2017) and westward (Gonzales et al., 1979; Kikuchi et al., 2003; Sastri et al., 2003; Sibeck et al., 1998) electric fields in the dayside low-latitudes ionosphere during substorms onset. In this study, two substorm events were identified during EMSTID observations, as indicated by AL index depletion (Figure 3b) and increased energetic particle (electron and proton) fluxes measured by geosynchronous satellite, LANL 1994-084, near magnetic midnight local time (Figure S1 in Supporting Information S1).

During the first substorm's expansion/recovery phases on 17 March (onset at 12:42:00 UT), h'F at Wakkanai showed no significant variation compared to geomagnetically quiet nights (Figures 3b and 3c). Additionally, h'F at Wakkanai, Yamagawa, Okinawa, and Kokubunji showed inconsistent trends, with the first three exhibiting enhancements and Kokubunji showing a notable reduction (Figure 3d). These four ionosondes span from high to low latitudes region of Japan. These inconsistencies suggest that the first substorm did not drive large-scale F-layer altitude changes. Notably, significant changes in EMSTID amplitude with substorm's phases were also not visible (Figure 3d). The effect of wind on F-layer altitude variation is not considered as the meridional wind on 17 March 2003 was significantly smaller (Figure 2f).

In contrast, the second substorm (onset at 13:50:29 UT on 17 March) had a pronounced impact. h'f at all four stations showed a significant increase/decrease during expansion/recovery phases, which were absent on considered quiet nights at Wakkanai station (Figures 3b–3d). EMSTID amplitude also exhibited a clear enhancement/decrement with the substorm's expansion/recovery phases (Figures 3b and 3d). While h'F began to enhance around 14:00 UT and decreased around 14:30 UT across all stations, the EMSTID amplitude showed a corresponding increase from 13:58 UT and a decrease from 14:32 UT, respectively. The changes in h'F and EMSTID amplitude are not perfectly synchronous, likely due to the difference in data resolution, 15 min for h'F and 30 s for TEC. This nearly synchronized variation strongly suggests a direct influence of substorm-imposed electric fields on the mid-latitude ionosphere. Since h'F was close to 300 km at substorm onset over Wakkanai, Kokubunji, and Yamagawa, effects of chemical loss on the h'F variations are negligible (Bittencourt & Abdu, 1981). While h'F over Okinawa was slightly lower (~275 km), the consistent variations across all four stations aligned with substorm phases confirming that the substorm-imposed electric fields were the primary mechanism driving F-layer altitude fluctuations.

Before and after the second substorm onset (13:40–14:20 UT and 22:40–23:20 LT), negative IMF-Bz (i.e., positive y-component of interplanetary electric field) indicated a downward  $E \times B$  drift due to a westward PPEF, yet this effect was not evident in h'F variations (Figures 3a and 3d). Instead, transient eastward/westward electric fields during the substorm's expansion/recovery phases appear to be the dominant driver of F-layer altitude changes and EMSTID amplitudes.

Notably, the growth rate of the Perkins theory is proportional to  $|E_{\rm eff}| = |E_{DD} + U_{DD} \times B|$  (Equation 1), which is southeastward in our case. Additional eastward/westward electric field will enhance/reduce the resultant value of  $|E_{\rm eff}|$ , causing enhancement/reduction of growth rate. In addition, polarization electric field of EMSTID,  $E_P$  is proportional to  $|E_{\rm eff}|$  (Otsuka et al., 2007). Eastward/westward electric field during expansion/recovery phase of substorm probably caused EMSTID amplitude enhancement/reduction resulted from amplified/reduced  $E_P \times B$  drifts inside EMSTID wavefronts. The upward/downward drift calculated from the F-layer altitude variations observed by ionosondes was ~17 m/s. Equating 17/cos(D) with electrodynamical drift,  $(E \times B)/|B|^2$ , would correspond to an electric field of ~0.8 mV/m. Therefore, the magnitude of electric fields imposed by the substorm was ~0.8 mV/m.

This study provides new insights into the long-debated role of substorm electric fields in mid-latitude ionospheric dynamics. Most importantly, our findings demonstrate the instantaneous modulation of EMSTID amplitudes by eastward/westward electric field during substorm's expansion/recovery phase. To our knowledge, the only prior study reporting such an effect is Rathi et al. (2025). Unlike our observations, they reported observations of electric fields of single polarity during each substorm with a delayed response of EMSTID amplitudes to substorm onset.

PATGIRI ET AL. 8 of 11



### 5. Conclusion

We report an observation of unusually aligned (NE-SW) EMSTID in detrended TEC maps over Japan on 17 March 2003 after two moderate storms. The following are the key findings:

- 1. The quiet-time dynamo electric field and neutral wind in the F-region, which are essential for developing the Perkins instability and generating typically aligned (NW-SE) EMSTIDs, cannot explain the unusual alignment of the observed EMSTID.
- 2. Eastward DDEF and westward wind helped in developing Perkins instability to generate NE-SW aligned EMSTID during the recovery phase of the storm.
- 3. Perkins instability can sufficiently be enhanced to generate EMSTIDs, even when E–F region coupling is weak in both hemispheres.
- 4. F-layer altitudes and EMSTID amplitudes were modulated instantaneously in response to the penetration of eastward/westward electric field during expansion/recovery phase of the second substorm. This result indicates that EMSTID amplitudes respond instantaneously to the direction and intensity change in the background electric fields.

### **Conflict of Interest**

The authors declare no conflicts of interest relevant to this study.

# **Data Availability Statement**

GPS TEC data is available at https://aer-nc-web.nict.go.jp/GPS/GEONET/. Ionosonde data sets for stations in Japan and Australia are available at https://wdc.nict.go.jp/Ionosphere/en/archive/ and https://www.sws.bom.gov.au/World\_Data\_Centre/1/3, respectively. Geomagnetic indices, solar and geophysical activity information, solar wind parameters and ROCSAT-1 data, and CHAMP data sets are available at https://wdc.kugi.kyoto-u.ac.jp/, https://www.spaceweatherlive.com/en/archive/.html, https://cdaweb.gsfc.nasa.gov/, and https://thermosphere.tudelft.nl/, respectively. All these data sets are available at Patgiri (2025).

### Acknowledgments

DP acknowledges support from ISEE, Nagoya University, Nagoya, Japan, during his visit as a visiting scholar. DP acknowledges the fellowship from the Ministry of Education, Government of India, for carrying out this research work at IIT Roorkee, Uttarakhand. This work is supported by JSPS KAKENHI (Grants 22K21345, 21H04518, and 20H00197), JSPS Bilateral Joint Research Projects JPJSBP120247202, JSPS Core-to-Core Program, B. Asia-Africa Science Platforms, and Humanosphere Science Research of RISH, Kyoto University.

### References

Bittencourt, J. A., & Abdu, M. A. (1981). A theoretical comparison between apparent and real vertical ionization drift velocities in the equatorial F region. *Journal of Geophysical Research*, 86(A4), 2451–2454. https://doi.org/10.1029/JA086iA04p02451

Blanc, M., & Richmond, A. D. (1980). The ionospheric disturbance dynamo. *Journal of Geophysical Research*, 85(A4), 1669–1686. https://doi.org/10.1029/JA085iA04p01669

Chakrabarty, D., Rout, D., Sekar, R., Narayanan, R., Reeves, G. D., Pant, T. K., et al. (2015). Three different types of electric field disturbances affecting equatorial ionosphere during a long-duration prompt penetration event. *Journal of Geophysical Research: Space Physics*, 120(6), 4993–5008. https://doi.org/10.1002/2014ja020759

Chakrabarty, D., Sekar, R., Narayanan, R., Devasia, C. V., & Pathan, B. M. (2005). Evidence for the interplanetary electric field effect on the oi 630.0 nm airglow over low latitude. *Journal of Geophysical Research*, 110(A11), A11301. https://doi.org/10.1029/2005JA011221

Chakrabarty, D., Sekar, R., Sastri, J. H., Pathan, B. M., Reeves, G. D., Yumoto, K., & Kikuchi, T. (2010). Evidence for oi 630.0 nm dayglow variations over low latitudes during onset of a substorm. *Journal of Geophysical Research*, 115(A10), A10316. https://doi.org/10.1029/2010JA015643

Cosgrove, R. B., & Tsunoda, R. T. (2002). A direction-dependent instability of sporadic-E layers in the nighttime midlatitude ionosphere. Geophysical Research Letters, 29(18), 11-1–11-4. https://doi.org/10.1029/2002GL014669

Ding, F., Wan, W., Xu, G., Yu, T., Yang, G., & Wang, J. (2011). Climatology of medium-scale traveling ionospheric disturbances observed by a GPS network in central China. *Journal of Geophysical Research*, 116(A9), A09327. https://doi.org/10.1029/2011ja016545

Duly, T. M., Chapagain, N. P., & Makela, J. J. (2013). Climatology of nighttime medium-scale traveling ionospheric disturbances (MSTIDs) in the central Pacific and South American sectors. Annales de Geophysique, 31(12), 2229–2237. https://doi.org/10.5194/angeo-31-2229-2013

Emmert, J. T., Fejer, B. G., Shepherd, G. G., & Solheim, B. H. (2004). Average nighttime F region disturbance neutral winds measured by UARS WINDII: Initial results. *Geophysical Research Letters*, 31(22), L22807. https://doi.org/10.1029/2004GL021611

Farley, D. T. (1960). A theory of electrostatic fields in the ionosphere at nonpolar geomagnetic latitudes. *Journal of Geophysical Research*, 65(3), 869–877. https://doi.org/10.1029/JZ065i003p00869

Fejer, B. G., Jensen, J. W., Kikuchi, T., Abdu, M. A., & Chau, J. L. (2007). Equatorial ionospheric electric fields during the November 2004 magnetic storm. *Journal of Geophysical Research*, 112(10), 1–11. https://doi.org/10.1029/2007JA012376

Fejer, B. G., Jensen, J. W., & Su, S. Y. (2008). Seasonal and longitudinal dependence of equatorial disturbance vertical plasma drifts. *Geophysical Research Letters*, 35(20), 2–5. https://doi.org/10.1029/2008GL035584

Fejer, B. G., Larsen, M. F., & Farley, D. T. (1983). Equatorial disturbance dynamo electric fields. *Geophysical Research Letters*, 10(7), 537–540. https://doi.org/10.1029/GL010i007p00537

Fujiwara, H., & Miyoshi, Y. (2009). Global distribution of the thermospheric disturbances produced by effects from the upper and lower regions: Simulations by a whole atmosphere GCM. Earth Planets and Space, 61(4), 463–470. https://doi.org/10.1186/BF03353163

PATGIRI ET AL. 9 of 11



- Fuller-Rowell, T. J. (1995). The dynamics of the lower thermosphere. In R. M. Johnson & T. L. Killeen (Eds.), The upper mesosphere and lower thermosphere: A review of experiment and theory, geophysical monograph series (Vol. 87, pp. 23–36). American Geophysical Union. https://doi.org/10.1029/gm087p0023
- Fuller-Rowell, T. J., Codrescu, M. V., Moffett, R. J., & Quegan, S. (1994). Response of the thermosphere and ionosphere to geomagnetic storms. Journal of Geophysical Research, 99(A3), 3893–3914. https://doi.org/10.1029/93JA02015
- Garcia, F. J., Kelley, M. C., Makela, J. J., & Huang, C. S. (2000). Airglow observations of mesoscale low-velocity traveling ionospheric disturbances at midlatitudes. *Journal of Geophysical Research*, 105(A8), 18407–18415. https://doi.org/10.1029/1999ja000305
- Gonzales, C., Kelley, M., Fejer, B., Vickrey, J., & Woodman, R. (1979). Equatorial electric fields during magnetically disturbed conditions: 2. Implications of simultaneous auroral and equatorial measurements. *Journal of Geophysical Research*, 84(A10), 5803–5812. https://doi.org/10.1029/JA084iA10p05803
- Gonzalez, W. D., Joselyn, J. A., Kamide, Y., Kroehl, H. W., Rostoker, G., Tsurutani, B. T., & Vasyliunas, V. M. (1994). What is a geomagnetic storm? *Journal of Geophysical Research*, 99(A4), 5771–5792. https://doi.org/10.1029/93JA02867
- Gonzalez, W. D., Tsurutani, B. T., Gonzalez, A. L. C., Smith, E. J., Tang, F., & Akasofu, S. I. (1989). Solar wind-magnetosphere coupling during intense magnetic storms (1978–1979). *Journal of Geophysical Research*, 94(A7), 8835–8851. https://doi.org/10.1029/JA094iA07p08835
- Hamza, A. M. (1999). Perkins instability revisited. Journal of Geophysical Research, 104(A10), 22567–22575. https://doi.org/10.1029/1999IA900307
- Hedin, A. E., Fleming, E. L., Manson, A. H., Schmidlin, F. J., Avery, S. K., Clark, R. R., et al. (1996). Empirical wind model for the upper, middle and lower atmosphere. *Journal of Atmospheric and Terrestrial Physics*, 58(13), 1421–1447. https://doi.org/10.1016/0021-9169(95)00122-0
- Huang, C. S. (2009). Eastward electric field enhancement and geomagnetic positive Bay in the dayside low-latitude ionosphere caused by magnetospheric substorms during Sawtooth events. Geophysical Research Letters, 36(18), 1–5. https://doi.org/10.1029/2009GL040287
- Huang, C.-S., Le, G., & Reeves, G. D. (2004). Periodic magnetospheric substorms during fluctuating interplanetary magnetic field B<sub>Z</sub>: Geophysical Research Letters, 31, L14801. https://doi.org/10.1029/2004GL020180
- Huang, C. S., Miller, C. A., & Kelley, M. C. (1994). Basic properties and gravity wave initiation of the mid-latitude F region instability. *Radio Science*, 29(1), 395–405. https://doi.org/10.1029/93RS01669
- Hui, D., Chakrabarty, D., Sekar, R., Reeves, G. D., Yoshikawa, A., & Shiokawa, K. (2017). Contribution of storm time substorms to the prompt electric field disturbances in the equatorial ionosphere. *Journal of Geophysical Research: Space Physics*, 122(5), 5568–5578. https://doi.org/ 10.1002/2016JA023754
- Hunsucker, R. (1982). Atmospheric gravity waves generated in the high-latitude ionosphere: A review. *Reviews of Geophysics*, 20(2), 293–315. https://doi.org/10.1029/RG020i002p00293
- Kelley, I. J., Kunduri, B. S. R., Baker, J. B. H., Ruohoniemi, J. M., & Shepherd, S. G. (2023). Storm time electrified MSTIDs observed over mid-latitude North America. *Journal of Geophysical Research: Space Physics*, 128(3), e2022JA031115. https://doi.org/10.1029/2022JA031115
- Kelley, M., Makela, J. J., Vlasov, M. N., & Sur, A. (2003). Further studies of the Perkins stability during space weather month. *Journal of Atmospheric and Solar-Terrestrial Physics*, 65(10), 1071–1075. https://doi.org/10.1016/j.jastp.2003.07.001
- Kelley, M. C., & Makela, J. J. (2001). Resolution of the discrepancy between experiment and theory of midlatitude F-region structures. Geophysical Research Letters, 28(13), 2589–2592. https://doi.org/10.1029/2000GL012777
- Kelley, M. C., Makela, J. J., Chau, J. L., & Nicolls, M. J. (2003). Penetration of the solar wind electric field into the magnetosphere/ionosphere system. Geophysical Research Letters, 30(4), 1158. https://doi.org/10.1029/2002GL016321
- Kikuchi, T., Hashimoto, K. K., Kitamura, T.-I., Tachihara, H., & Fejer, B. (2003). Equatorial counter electrojets during substorms. *Journal of Geophysical Research*, 108(A11), 1406. https://doi.org/10.1029/2003JA009915
- La Belle, J. (1985). Mapping of electric field structures from the equatorial F region to the underlying E region. *Journal of Geophysical Research*, 90, 4341–4346. https://doi.org/10.1029/JA090iA05p04341
- Liu, H., Lühr, H., Watanabe, S., Kühler, W., Henize, V., & Visser, P. (2006). Zonal winds in the equatorial upper thermosphere: Decomposing the solar flux, geomagnetic activity, and seasonal dependencies. *Journal of Geophysical Research*, 111, A07307. https://doi.org/10.1029/ 2005JA011415
- Liu, Y., Li, Z., Fu, L., Wang, J., & Zhang, C. (2020). Studying the ionospheric responses induced by a geomagnetic storm in September 2017 with multiple observations in America. GPS Solutions, 24(1), 3. https://doi.org/10.1007/s10291-019-0916-1
- Makela, J. J., & Otsuka, Y. (2012). Overview of nighttime ionospheric instabilities at low- and mid-latitudes: Coupling aspects resulting in structuring at the mesoscale. Space Science Reviews, 168(1–4), 419–440. https://doi.org/10.1007/s11214-011-9816-6
- Meriwether, J. W. (2008). Thermospheric dynamics at low and mid-latitudes during magnetic storm activity. *Geophysical Monograph Series*, 181, 201–219. https://doi.org/10.1029/181GM19
- Narayanan, V. L., Shiokawa, K., Otsuka, Y., & Neudegg, D. (2018). On the role of thermospheric winds and sporadic E layers in the formation and evolution of electrified MSTIDs in geomagnetic conjugate regions. *Journal of Geophysical Research: Space Physics*, 123(8), 6957–6980. https://doi.org/10.1029/2018JA025261
- Nishioka, M., Saito, A., & Tsugawa, T. (2009). Super-medium-scale traveling ionospheric disturbance observed at midlatitude during the geomagnetic storm on 10 November 2004. *Journal of Geophysical Research*, 114(A7), A07310. https://doi.org/10.1029/2008JA013581
- Otsuka, Y., Kotake, N., Shiokawa, K., Ogawa, T., Tsugawa, T., & Saito, A. (2011). Statistical study of medium-scale traveling ionospheric disturbances observed with a GPS receiver network in Japan. Aeronomy of the Earth's Atmosphere and Ionosphere, 291–299. https://doi.org/ 10.1007/978-94-007-0326-1\_21
- Otsuka, Y., Ogawa, T., Saito, A., Tsugawa, T., Fukao, S., & Miyazaki, S. (2002). A new technique for mapping of total electron content using GPS network in Japan. Earth Planets and Space, 54(1), 63–70. https://doi.org/10.1186/BF03352422
- Otsuka, Y., Onoma, F., Shiokawa, K., Ogawa, T., Yamamoto, M., & Fukao, S. (2007). Simultaneous observations of nighttime medium-scale traveling ionospheric disturbances and E region field-aligned irregularities at midlatitude. *Journal of Geophysical Research*, 112(A6), A06317. https://doi.org/10.1029/2005JA011548
- Otsuka, Y., Shinbori, A., Tsugawa, T., & Nishioka, M. (2021). Solar activity dependence of medium-scale traveling ionospheric disturbances using GPS receivers in Japan. Earth Planets and Space, 73(1), 1–11. https://doi.org/10.1186/s40623-020-01353-5
- Otsuka, Y., Tani, T., Tsugawa, T., Ogawa, T., & Saito, A. (2008). Statistical study of relationship between medium-scale traveling ionospheric disturbance and sporadic E layer activities in summer night over Japan. *Journal of Atmospheric and Solar-Terrestrial Physics*, 70(17), 2196–2202. https://doi.org/10.1016/j.jastp.2008.07.008
- Patgiri, D. (2025). Detrended total electron content data (Detrended\_TEC), CHAMP cross-track wind data (CHAMP\_Wind\_Data), ROCSAT-1 ion drift data (ROCSAT\_Data), ionosonde data for Japanese stations (ionosonde\_Data\_Japan), ionosonde data for Australian station (ionosonde\_Data\_Australia), solar wind parameters (solar\_Wind\_Parameter), AL index data (AL\_Index\_Data) [Dataset]. Zenodo. https://doi.org/10.5281/zenodo.15823746

PATGIRI ET AL. 10 of 11



- Perkins, F. (1973). Spread F and ionospheric currents. Journal of Geophysical Research, 78(1), 218-226. https://doi.org/10.1029/ia078i001p00218
- Perwitasari, S., Nakamura, T., Tsugawa, T., Nishioka, M., Tomikawa, Y., Ejiri, M. K., et al. (2022). Propagation direction analyses of medium-scale traveling ionospheric disturbances observed over North America with GPS-TEC perturbation maps by three-dimensional spectral analysis method. *Journal of Geophysical Research: Space Physics*, 127(1), e2020JA028791. https://doi.org/10.1029/2020ja028791
- Rathi, R., Sivakandan, M., Chakrabarty, D., Krishna, M. S., Upadhayaya, A. K., & Sarkhel, S. (2025). Evidence for the evolution and decay of an electrified medium scale traveling ionospheric disturbances during two consecutive substorms: First results. *Advances in Space Research*, 75(6), 4896–4909. https://doi.org/10.1016/j.asr.2025.01.007
- Reigber, C., Lühr, H., & Schwintzer, P. (2002). CHAMP mission status. Advances in Space Research, 30(2), 129–134. https://doi.org/10.1016/S0273-1177(02)00276-4
- Richmond, A. D. (2021). Joule heating in the thermosphere. In W. Wang (Ed.), *Upper atmosphere dynamics and energetics* (Vol. 4, pp. 3–18). https://doi.org/10.1002/9781119815631.ch1
- Rishbeth, H. (1971). The F-layer dynamo. Planetary and Space Science, 19(2), 263-267. https://doi.org/10.1016/0032-0633(71)90205-4
- Saito, A., Fukao, S., & Miyazaki, S. (1998). High resolution mapping of TEC perturbations with the GSI GPS network over Japan. *Geophysical Research Letters*, 25(16), 3079–3082. https://doi.org/10.1029/98GL52361
- Saito, S., Yamamoto, M., Hashiguchi, H., Maegawa, A., & Saito, A. (2007). Observational evidence of coupling between quasi-periodic echoes and medium scale traveling ionospheric disturbances. *Annals of Geophysics*, 25(10), 2185–2194. https://doi.org/10.5194/angeo-25-2185-2007
- Sastri, J. H., Kamide, Y., & Yumoto, K. (2003). Signatures for magnetospheric substorms in the geomagnetic field of dayside equatorial region: Origin of the ionospheric component. *Journal of Geophysical Research*, 108(A10), 1375. https://doi.org/10.1029/2003JA009962
- Shiokawa, K., Ihara, C., Otsuka, Y., & Ogawa, T. (2003). Statistical study of nighttime medium-scale traveling ionospheric disturbances using midlatitude airglow images. *Journal of Geophysical Research*, 108(A1), 1052. https://doi.org/10.1029/2002JA009491
- Shiokawa, K., Otsuka, Y., Ihara, C., Ogawa, T., & Rich, F. J. (2003). Ground and satellite observations of nighttime medium-scale traveling ionospheric disturbance at midlatitude. *Journal of Geophysical Research*, 108(A4), 1145. https://doi.org/10.1029/2002JA009639
- Sibeck, D. G., Takahashi, K., Yumoto, K., & Reeves, G. D. (1998). Concerning the origin of signatures in dayside equatorial ground magnetograms. *Journal of Geophysical Research*, 103(A4), 6763–6769. https://doi.org/10.1029/97JA03600
- Spreiter, J. R., & Briggs, B. R. (1961). Theory of electrostatic fields in the ionosphere at polar and middle geomagnetic latitudes. *Journal of Geophysical Research*, 66(6), 1731–1744. https://doi.org/10.1029/JZ066i006p01731
- Tsugawa, T., Otsuka, Y., Coster, A. J., & Saito, A. (2007). Medium-scale traveling ionospheric disturbances detected with dense and wide TEC
- maps over North America. Geophysical Research Letters, 34(22), L22101. https://doi.org/10.1029/2007GL031663
  Tsunoda, R. T., & Cosgrove, R. B. (2001). Coupled electrodynamics in the nighttime midlatitude ionosphere. Geophysical Research Letters,
- 28(22), 4171–4174. https://doi.org/10.1029/2001GL013245
  Tsurutani, B. T., Verkhoglyadova, O. P., Mannucci, A. J., Saito, A., Araki, T., Yumoto, K., et al. (2008). Prompt penetration electric fields (PPEFs) and their ionospheric effects during the great magnetic storm of 30-31 October 2003. *Journal of Geophysical Research*, 113(A5),
- A05311. https://doi.org/10.1029/2007JA012879

  Yokoyama, T. (2014). Hemisphere-coupled modeling of nighttime medium-scale traveling ionospheric disturbances. Advances in Space Research, 54(3), 481–488. https://doi.org/10.1016/j.asr.2013.07.048
- Yokoyama, T., Hysell, D. L., Otsuka, Y., & Yamamoto, M. (2009). Three-dimensional simulation of the coupled Perkins and Es-layer instabilities in the nighttime midlatitude ionosphere. *Journal of Geophysical Research*, 114(A3), A03308, https://doi.org/10.1029/2008IA013789
- Zhang, S.-R., Erickson, P. J., Coster, A. J., Rideout, W., Vierinen, J., Jonah, O. F., & Goncharenko, L. P. (2019). Subauroral and polar traveling ionospheric disturbances during the 7–9 September 2017 storms. Space Weather, 17(12), 1748–1764. https://doi.org/10.1029/2019SW002325
- Zhang, S.-R., Nishimura, Y., Erickson, P. J., Aa, E., Kil, H., Deng, Y., et al. (2022). Traveling ionospheric disturbances in the vicinity of storm-enhanced density at midlatitudes. *Journal of Geophysical Research: Space Physics*, 127(8), e2022JA030429. https://doi.org/10.1029/2022JA030429

PATGIRI ET AL.